

Article

Influence of Temperature and Moisture Content on Thermal Performance of Green Roof Media

Bohan Shao ¹, Caterina Valeo ¹ , Phalguni Mukhopadhyaya ^{2,*}  and Jianxun He ³ 

¹ Mechanical Engineering, University of Victoria, Victoria, BC V8W 2Y2, Canada; bohanwins@gmail.com (B.S.); valeo@uvic.ca (C.V.)

² Civil Engineering, University of Victoria, Victoria, BC V8W 2Y2, Canada

³ Civil Engineering, Schulich School of Engineering, University of Calgary, Calgary, AB T2N 1N4, Canada; jianhe@ucalgary.ca

* Correspondence: phalguni@uvic.ca

Abstract: The influence of moisture content on substrate thermal conductivity at different temperatures was investigated for four different commercially available substrates for green roofs. In the unfrozen state, as moisture content increased, thermal conductivity increased linearly. In the phase transition zone between +5 and −10 °C, as temperature decreased, thermal conductivity increased sharply during the transition from water to ice. When the substrate was frozen, thermal conductivity varied exponentially with substrate moisture content prior to freezing. Power functions were found between thermal conductivity and temperature. Two equally sized, green roof test cells were constructed and tested to compare various roof configurations including a bare roof, varying media thickness for a green roof, and vegetation. The results show that compared with the bare roof, there is a 75% reduction in the interior temperature's amplitude for the green roof with 150 mm thick substrate. When a sedum mat was added, there was a 20% reduction in the amplitude of the inner temperature as compared with the cell without a sedum mat.

Keywords: green roof; thermal conductivity; moisture content; heat flow meter; thermal performance; frozen soils



Citation: Shao, B.; Valeo, C.; Mukhopadhyaya, P.; He, J. Influence of Temperature and Moisture Content on Thermal Performance of Green Roof Media. *Energies* **2021**, *14*, 2421. <https://doi.org/10.3390/en14092421>

Academic Editor: Wahid Maref

Received: 21 March 2021

Accepted: 19 April 2021

Published: 23 April 2021

Publisher's Note: MDPI stays neutral with regard to jurisdictional claims in published maps and institutional affiliations.



Copyright: © 2021 by the authors. Licensee MDPI, Basel, Switzerland. This article is an open access article distributed under the terms and conditions of the Creative Commons Attribution (CC BY) license (<https://creativecommons.org/licenses/by/4.0/>).

1. Introduction

There is growing concern for global energy consumption due to the adverse environmental impacts, insufficient energy resources, difficulties in supply, and economic growth [1]. Among all the energy consumption sectors, the building sector is one of the largest sectors and contributed to 32% of energy consumption used globally in 2010 and contributed to one third of greenhouse gases [2,3]. Green roofs are becoming a prevalent development option for buildings and are considered to have good potential for decreasing the building indoor cooling and heating loads. Green roofs also have numerous environmental, social, and economic benefits as well. Research has shown that green roofs can reduce stormwater runoff and the urban heat island effect, provide habitat for wildlife, enhance air and water quality, reduce the energy consumption of buildings, and reduce noise pollution [4–6]. A green roof is a roof that is covered with a growing medium (the substrate layer), vegetation, as well as other functional layers (e.g., drainage layer and filter layer) [7]. Among all the layers of a green roof, the vegetation layer and the substrate layer are the most important layers; thus, they need to be strategically selected to maximize the many benefits of a green roof.

The substrate layer plays an important role in water runoff reduction, peak flow reduction, water quality improvement, and thermal benefits. Based on the thickness of the substrate, a green roof can be divided into three categories: intensive (above 12 inch or 30 cm), semi-intensive (6–12 inch or 15–30 cm), and extensive (3–6 inch or 8–15 cm) [4,8]. The intensive green roof has a higher water holding capacity and more plant options

including small trees and shrubs; however, this requires more maintenance, irrigation, fertilization, as well as more consideration to building structural support. Compared with the intensive green roof, the extensive green roof is more common globally because of its low maintenance, nutrient and irrigation requirements.

The vegetation layer plays an important role in improving runoff water quality [9], reducing heating effects [10], and providing animal habitat. In the selection of vegetation, geographic location, wind, humidity, temperature, rainfall, and sun exposure should all be considered while noting that the choice of plant species is also influenced by the designed soil thickness. Many studies have focused on the selection of suitable plants [11,12], with most agreeing that sedum species are good options for extensive green roofs all over the world, since they can survive under a variety of conditions. Teeri et al. [13] indicated that *Sedum rubrotinctum* R. T. Clausen can survive for 2 years without water, while Durhman et al. [14] indicated that *Sedum* can survive and maintained active photosynthetic metabolism after 4 months without water. Succulents can also survive through droughts because they store water in their stems and leaves [15].

Many studies have investigated the energy performance of vegetated green roofs. Vera et al. [16] studied the influence of an extensive green roof on the retail stores' thermal performance using EnergyPlus 8.6.0 (NREL, Department of Energy, Washington DC, MD, USA). Mahmoodzadeh et al. [3] studied the effects of green roofs on school buildings energy performance using EnergyPlus 8.8. Both studies note limitations in the EnergyPlus program, such as the fact that substrate moisture content varies over time, but substrate thermal properties are held constant over time. These result in a lack of accuracy in substrate thermal properties that are input to the model. In general, these approaches are plagued by a variety of problems including inaccuracy in model inputs of substrate thermal properties and lack of knowledge of the role of the substrate separate from the vegetation. Regarding the lack of accuracy in substrate thermal properties that are input to the models, it is well known that substrate thermal properties such as thermal conductivity, specific heat capacity, albedo play important roles in soil energy balance. Those parameters are influenced by substrate density, porosity, temperature, and in particular, moisture content. The substrate's density and porosity are substrate specific and may be indirectly related to temperature and moisture content. While, the temperature and moisture content are a function of the weather and environmental conditions, irrespective of the substrate.

Low porosity makes heat transfer through the substrate easier because the particles are compressed tighter, resulting in a greater number of interior contact points that aid higher conduction heat transfer [17,18]. Soil thermal performance varies as moisture content changes because water will replace the air among soil particles and connects the gaps between them [19]. Temperature also plays an important role in thermal performance, especially in the phase transition zone [20]. According to the energy balance study of green roof, substrate parameters that are critical to green roof energy budget are density, thermal conductivity, specific heat capacity, emissivity, and albedo. Pianella et al. [6] noted that many studies that were analyzing variations in thermal conductivity, did so using transient measurements. Transient measurements are made when the measurand, or factors affecting the measurand, vary with time [6]; which can give rise to uncertainty and error. In steady-state observations on the other hand, the measurand has reached an equilibrium or steady-state condition in which the measurand or influencing factors, do not change over time. This gives rise to consistent observations necessary for modeling and inference. Pianella et al. [6] compared transient vs. steady-state measurement and found that steady-state measurements are more consistent within replicates and provides more accurate results as compared with transient measurements.

As noted, there is a lack of information and research on the energy performance of the substrate alone. Although many researchers have studied the thermal and energy performance of green roofs, very few have focused on the performance of the substrate in isolation. This would be important in many climates in which the vegetation is inactive or less active in energy and water budgets for a portion of the year. In the fall and winter

months, which is the case in many parts of Canada, the substrate is the only “active” layer year-round, and may undergo freezing and thus, its thermal conductivity may change with temperature and moisture content prior to freezing. There is a lack of studies on the thermal performance of the substrate in isolation, particularly during freeze–thaw periods. Therefore, further understanding the substrates’ role in the energy and water budget of a green roof in these periods requires isolating the substrate layer from the vegetation layer in any numerical or experimental study. This will provide insight to improving estimates of the parameters used to model energy and moisture budgets in green roof systems.

Many parts of Canada are exploring or adopting green roof technology through either retrofitting old buildings with green roofs or installing green roofs on new buildings [21]. In Toronto, Ontario, Canada, for example, the relevant by-law required new buildings larger than 2000 m² to green 20–60% of the building rooftop [21]. As green roofs are increasing in popularity due to the numerous environmental, social, and economic benefits, design methodologies that can realistically achieve the benefits afforded by this technology are being sought for application in all Canadian climates. Therefore, to better support the design process given the literature review above, the objective of this research is to study the thermal performance of the substrate in a green roof as it is affected by temperature and moisture content. An experiment into the thermal conductivity at different temperatures and moisture contents was performed using four different commercially available substrates for green roofs. Additionally, experiments on two equally sized, experimental green roof test cells constructed in Victoria, BC were used to investigate the thermal performance of substrate and green roof related design parameters in an outdoor environment. The substrates examined are specifically available and proposed for use in Canadian climates. The lab experiments will provide users information on aspects unique to these substrates and results will be compared to other studies using similar substrates that are looking at the role of moisture content on thermal conductivity. This will also support parameterization of these substrates in energy models. The outdoor experiments will further explore the use of these substrates in green roofs for modifying interior temperatures. These experiments will also support an unconventional modeling approach in which the green roofs studied are modeled as first-order dynamic systems that respond to exterior temperatures depending on the roof’s condition (determined by factors including moisture content, substrate, roof design, vegetation and irrigation). By determining and comparing the time constants of each first-order system, more definitive conclusions can be drawn on the role of these influencing factors on the green roof’s role in energy budgeting.

2. Materials and Methods

2.1. Thermal Conductivity Experimental Study

Four different commercially available substrates for green roofs (Sopraflor I, Sopraflor X, Zinco Blend and Eagle Lake) were used in this study. These substrates are being used by organizations installing green roofs in regions of Canada that experience cold climates, like the province of Alberta. Samples of the substrates were obtained through collaborations with the University of Calgary and the City of Calgary. The Sopraflor I and Sopraflor X has mineral aggregates, blond peat, perlite, sand and compost from vegetable matter as soil components. The soil components of Zinco Blend include high-quality recycled materials and minerals enhanced with high-quality compost, while Eagle Lake substrate is composed of peat moss, fir bark fines, compost, sand, pumice and perlite.

Sample Preparation

To study substrate thermal conductivity as a function of temperature and moisture content, the four substrates were tested under different temperatures and moisture contents. Temperature varied from −10 to 35 °C with an interval of 15 °C. This variation is based on Calgary and Victoria’s outdoor air temperature. Calgary is a semiarid, prairie city in southern Alberta, Canada. Victoria is located on the southern tip of Vancouver Island

which has a warm-summer Mediterranean climate [22]. Moisture content was varied from dry substrate up to saturation with an interval of 10% moisture content by mass. Substrates were dried in an oven at 104 °C for 48–72 h as recommended in ASTM E2399-05 [23]. Once the mass difference between the last two measurements over the mass of the final substrate is less than 1%, the substrate is assumed to be dry. The wet substrate was prepared at each wetness interval by adding water with a mass of 10% of the dry substrate. The sample was mixed well and allowed to settle overnight before being tested.

To determine the thermal conductivity of substrates using a heat flow meter, a sample frame was constructed from pinewood [24] (thermal conductivity of 0.106 W/m·K) with a paper-based phenolic board with a thickness of 1.6 mm and thermal conductivity of 0.12 W/m·K for the base. The overall dimensions were 293 × 293 × 45.6 mm. The material and dimensions were determined based on ASTM C687-18 [24] and the Heat Flow Meter NETZSCH HFM 436/3/1E. The dry/wet substrate was then poured into the holding frame. A 14 kg cylindrical mold with a diameter of 150 mm was applied at different positions of the substrate top surface. Each position was applied for 2 min and a 2.5 kg manual rammer was dropped from a height of 150 mm five times at each position for greater compression. This compaction method was based on ASTM D698-07 [25].

According to Clarke [26], for samples with thermal resistance lower than 1.0 m²·K/W, the most significant error may come from interface resistance. ASTM C518 [27] also suggests for the sample in which it is hard to obtain good surface contact between the sample and the testing plate, a thin sheet of suitable homogeneous material could be used between the sample and the plate surfaces. Since the surface of substrates used in this test is uneven, which may result in a high interface resistance, a buffer sheet was used to minimize the influence of interface resistance. Clarke used four different buffer sheet materials to perform the test and found silicone sponge provided the most uniform results. In this experiment, a silicone sponge with the thickness of 9 mm was used as a buffer and one was placed on the top surface of the substrate and a second one on the bottom. The buffer sheets were slightly compressed during the test to perform good contact with the substrate surface as well as the bottom frame.

In this study, HFM 436/3/1E was used to test the thermal conductivity of four substrates. Heat Flow Meter is an apparatus to determine thermal conductivity through a process of steady-state measurements [28]. The test sample is in contact with hot and cold plates that have two different stable temperatures. Heat flows vertically from the upper, hot plate to the lower, cold plate through the test sample and sensors on the plates measure temperature and heat flux once per minute until all readings stabilize. The thermal conductivity of the test sample under steady-state conditions is calculated. The average temperature is the average of the hot and cold plate temperatures. The test sample is the loose fill substrate, together with the buffer sheet and the holding frame. The test results are thermal conductivity and thermal resistance of the whole test sample. To achieve substrate thermal conductivity, a reference sample is also measured. The test sample and the reference sample setup are shown in Figure 1a. Cling wrap was also included in both the test and reference samples, but it is very thin, and thermal resistance can be neglected.

According to Clarke [29], the total test sample thermal resistance is:

$$R_t^1 = R_{b1} + R_{b1-s} + R_s + R_{s-f} + R_f + R_{f-b2} + R_{b2} \quad (1)$$

where R_t^1 is the total test sample thermal resistance; R_{b1} is the upper buffer sheet thermal resistance; R_{b1-s} is the interface thermal resistance between the upper buffer sheet and the substrate; R_s is the substrate thermal resistance; R_{s-f} is the interface thermal resistance between substrate and base frame; R_f is the base frame thermal resistance; R_{f-b2} is the interface thermal resistance between base frame and lower buffer sheet; R_{b2} is the lower buffer sheet thermal resistance. The total reference sample thermal resistance is:

$$R_t^2 = R_{b1} + R_{b1-f} + R_f + R_{f-b2} + R_{b2} \quad (2)$$

where R_{b1-f} is the interface thermal resistance between the upper buffer sheet and the base frame. By subtracting these two thermal resistances, the resistance difference is:

$$R_{diff} = R_t^1 - R_t^2 = R_{b1-s} + R_s + R_{s-f} - R_{b1-f} \quad (3)$$

Both R_{b1-s} and R_{b1-f} are mediated by layers of cling wrap and these two resistances should cancel. R_{s-f} is the interface thermal resistance between the substrate's bottom surface and the base frame top surface. As the substrate and holding frame were prepared and allowed to settle overnight, this led to uniform contact between the substrate and holding frame and, therefore, this resistance should be very small. Thus, $R_{diff} = R_s$, and the substrate thermal conductivity k_s (W/m·K) is calculated as:

$$k_s = \frac{d_s}{R_s} \quad (4)$$

where d_s is substrate thickness (m) and R_s is in $m^2 \cdot K/W$.

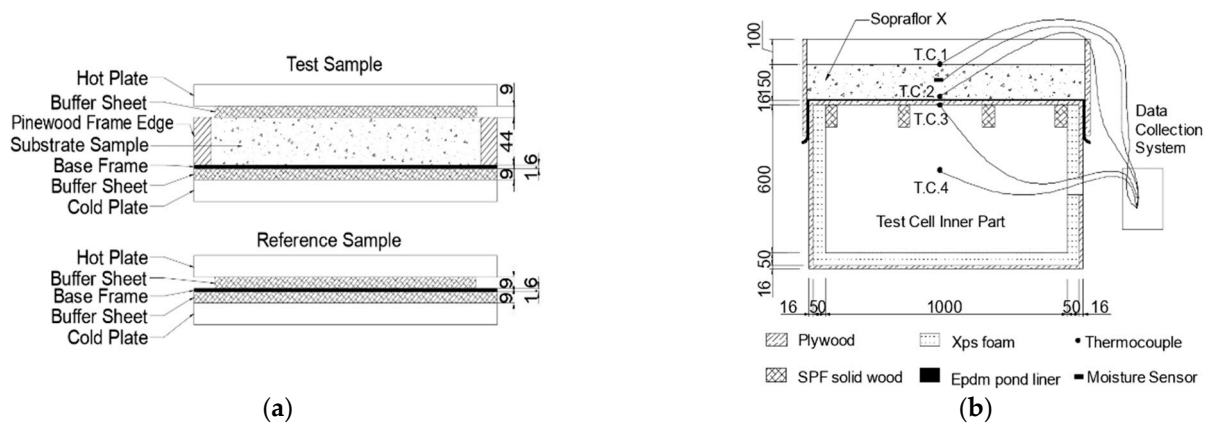


Figure 1. (a) Test sample and reference sample arrangement (dimensions in mm); (b) experimental test cell with 150 mm thickness Sopraflor X (dimensions in mm).

2.2. Outdoor Environment Study

To further analyze the thermal performance of the substrate layer in an uncontrolled environment, two equally sized experimental test cells were constructed for testing outdoors in Victoria, BC, Canada. Figure 1b shows the experimental test cell setup. The test cell consists of a six-wall enclosure with inner dimensions of $1 \times 1 \times 0.6$ m (height), constructed using 0.016 m thick plywood. Except for the top surface, the inner sides of the other five surfaces were insulated with 0.05 m thick XPS foam, with $10 m^2 \cdot K/W$ thermal resistance. Four SPF solid wood vertical supports were used on the inner side of the top surface to provide support for the substrate. To prevent water from entering into the test cell, a layer of EPDM pond liner was used above the test cell top surface. The Sopraflor X substrate was then poured on the EPDM pond liner until it reached the predetermined thicknesses of 150 (extensive) and 200 mm (intensive) for the experiment. As shown in Figure 1b, for each test cell, four thermocouples HOBO E348-TMC50-HD with accuracy of ± 0.25 °C were located at the surface of the substrate (T.C.1), under the substrate layer, on the surface of EPDM pond liner (T.C.2), at the roof's inner plywood ceiling surface (T.C.3), and in the center of test cell (T.C.4). All are programmed to read temperature every minute at each location. For each test cell, a moisture sensor Delta ML3 Theta Probe was located inside the substrate to read the substrate moisture content every 2 min. Data loggers HOBO E348-U12-008 and Delta E312-GP1 were used to record data.

Images of the two experimental test cells located at the University of Victoria campus are shown in Figure 2. The test cells surfaces were painted white to reflect solar radiation that could enter through the side walls. Two cells were set up with a mild slope to avoid

water accumulation on the roof. To avoid the influence of test cell and shed shadow, and to ensure they experienced the same weather conditions, the distance between them and the distance between the test cells and the shed were determined by shadow length simulation results obtained from the Suncalc website (<https://www.suncalc.org/> (accessed on 1 March 2019)). There is an access door on one side of the test cell to allow access to the interior. The door was also insulated with XPS foam, sealed with rubber weatherseal, and screwed tightly to minimize the heat transfer through the door. The access door was covered by the EPDM pond liner to prevent water from entering but the pond liner was not attached to the access door very tightly. An air gap between them was created so that the solar energy absorbed by the pond liner would not transfer effectively to the access door. Holes permitting cables were also insulated and waterproofed. Several tests were performed from May to August 2019. Table 1 shows the schedule and model for each test.



Figure 2. (a) Two experimental test cells; (b) cables routing from inside; (c) green roof test cell surface (d) bare roof test cell surface; (e) roof with 150 mm thick substrate test cell surface.

Table 1. Test schedule.

Test Number	Date (2019)	Description	Test Cell A	Test Cell B
1	9–15 July	Influence of substrate layer	Bare roof	Roof +150 mm Sopraflor X
2	30 May–2 June	Influence of substrate layer thickness	Roof + 150 mm Sopraflor X	Roof + 200 mm Sopraflor X
3	2–8 July	Influence of moisture content	Roof + 150 mm soil No irrigation	Roof + 150 mm soil with irrigation
4	7–13 August	Influence of vegetation layer	Roof + 150 mm Sopraflor X	Roof + 150 mm Sopraflor X + Sedum

To analyze the impact of the substrate layer, substrate thickness and vegetation layer on green roof thermal performance, comparisons were made for the bare roof (no vegetation

and substrate layer, as shown Figure 2d), vs. roof with 150 mm thick substrate (as shown in Figure 2e); roof with 150 mm thick substrate vs. roof with 200 mm thick substrate; roof with 150 mm thick substrate vs. roof with 150 mm thick substrate and vegetation layer (as shown in Figure 2c).

3. Results and Discussions

3.1. Results of Thermal Conductivity Experimental Study

3.1.1. Dry Substrate Density

The physical properties of four substrates are shown in Table 2. Sopraflor I has the lowest dry density, which is 865.1 kg/m^3 due to the high percentage of high porous mineral aggregate, with 1.75 mm D50 average particle size [30]. Eagle Lake has the highest dry density, which is 1184.1 kg/m^3 due in part to high percentage of sand, with 0.8575 mm D50 average particle size. These characteristics contribute to the reasons why Sopraflor I has the highest moisture holding capacity by mass and Eagle Lake has the lowest.

Table 2. Physical properties of the four tested substrates.

Substrate	Sopraflor I	ZincoBlend	Sopraflor X	Eagle Lake
Dry density (kg/m^3)	856.1	921.9	1022.8	1184.1
Moisture holding capacity	50~60%	40~50%	30~40%	30~40%

Figure 3 shows the substrates' thermal conductivities at different temperatures and moisture contents. From the figure we can see that no matter the temperature or moisture content, Eagle Lake always has the highest thermal conductivity, while Sopraflor I always has the lowest. It appears, based on the results available from this study, irrespective of temperature or moisture content, the substrate with the higher dry density exhibits the higher thermal conductivity. With average particle size D50 of 0.8575 mm, Eagle Lake particles are compressed tighter as compared with Sopraflor I (D50 of 1.75 mm) which makes it easier for heat to transfer through the substrate. Figure 3 indicates that dry density has a significant influence on the substrate thermal conductivity.

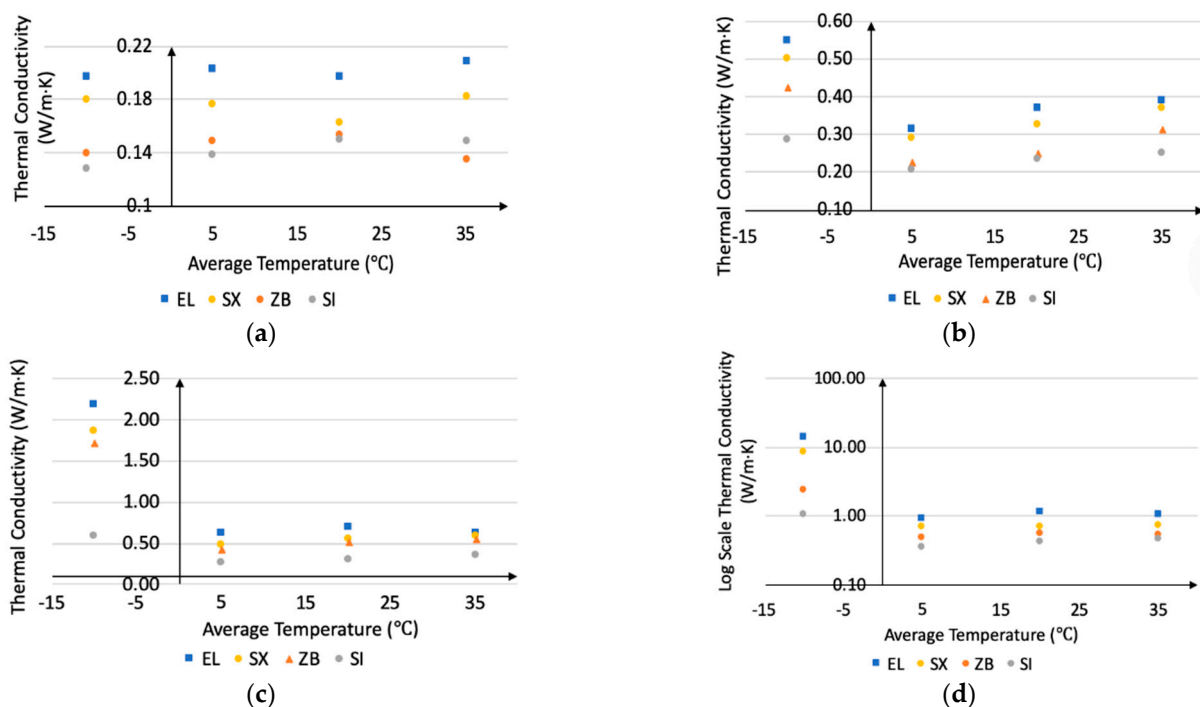


Figure 3. Thermal conductivity vs. average temperature for (a) dry substrates; (b) substrates with 10% MCM; (c) substrates with 20% MCM; (d) substrates with 30% MCM.

3.1.2. Moisture Content

Figure 4 shows the variation of four substrates thermal conductivities with moisture content under different average temperatures. Fitting functions to the data taken in the unfrozen and frozen states are shown in Table 3. It can be seen from the figure and table that moist soil is more conductive compared with dry soil. This is because water replaced the air among soil particles and connects the gaps between them, which increase the contact area. In the unfrozen state (5, 20 and 35 °C), as shown in Figure 4a–c, thermal conductivity increases linearly as moisture content increases. Best fit functional forms were linear in the unfrozen state and exponential in the frozen state. The coefficients of determination (R^2) values are also shown in Table 3. As substrate density increases, the slope of fitting function increases. Eagle Lake (dry density 1184.1 kg/m³) thermal conductivity shows the most significant increase (with a linear slope of 2.33–3.04) as moisture increases, whereas Sopraflor I (dry density 856.1 kg/m³) thermal conductivity shows the smallest increase (with a slope of 1.09–1.15). This is because a larger amount of water is added to the Eagle Lake substrate.

In the frozen state (−10 °C) as shown in Figure 4d, an exponential function exists between thermal conductivity and moisture content. Thermal conductivity increases more sharply as substrate moisture content prior to freezing increases in the frozen state than in the unfrozen state. This is because the thermal conductivity of ice is much larger than that of water. As substrate dry density increases, the slope and index of the fitting function increases.

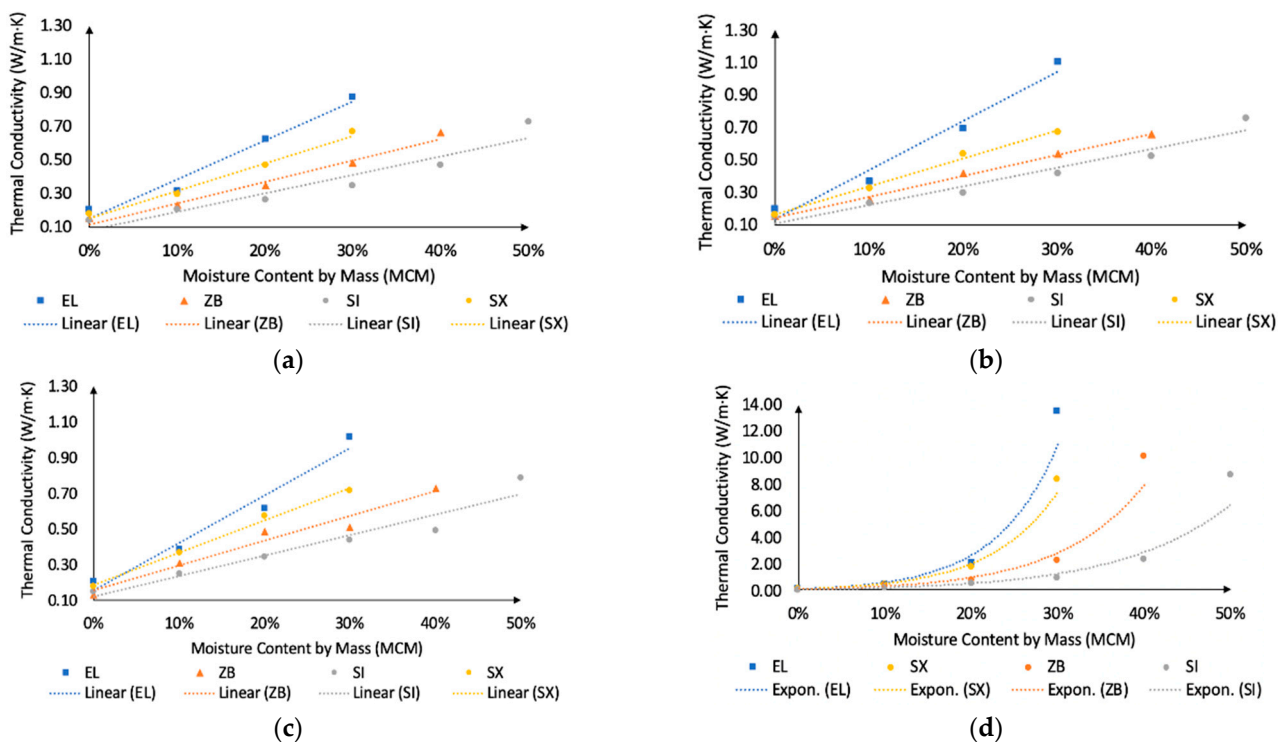


Figure 4. Substrates' thermal conductivity vs. moisture content by mass at average temperature of (a) 5 °C; (b) 20 °C; (c) 35 °C; (d) −10 °C.

Table 3. Thermal conductivity y (W/m·K) as a function of moisture content (x) by mass of the form $y = mx + b$ where m is the slope and b is the constant. Where the relationship is nonlinear, the complete function is given.

		5 °C	20 °C	35 °C	−10 °C
Sopraflor I (SI)	m	1.09	1.15	1.15	$y = 0.12e^{8.03x}$
	b	0.08	0.11	0.12	
	R^2	0.91	0.95	0.93	
Zinco Blend (ZB)	m	1.27	1.30	1.39	$y = 0.13e^{10.25x}$
	b	0.12	0.14	0.16	
	R^2	0.98	0.99	0.96	
Sopraflor X (SX)	m	1.64	1.74	1.82	$y = 0.16e^{12.86x}$
	b	0.15	0.16	0.19	
	R^2	0.98	0.99	0.99	
Eagle Lake (EL)	m	2.33	3.04	2.66	$y = 0.16e^{14.08x}$
	b	0.16	0.13	0.16	
	R^2	0.98	0.97	0.96	

3.1.3. Average Temperature

Figure 5 shows the variation of four substrates' thermal conductivities with average temperature under different moisture content. The figure illustrating data in the unfrozen state (5, 20 and 35 °C) shows that it is difficult to see a relationship between thermal conductivity and average temperature. To further analyze the relationship between these data, the Mann–Kendall Trend Test was used to analyze the relationship between thermal conductivity and average temperature in the unfrozen state. Results showed that for all four substrates under different moisture contents, there is no significant relationship between thermal conductivity and average temperature in the unfrozen state. In the phase transition zone (between −10 and 5 °C), as average temperature decreases, thermal conductivity increases sharply during the transition from water to ice. This is because the thermal conductivity of ice is much larger than that of water. Additionally, during the phase transition zone, soil structure changed because of the sharp transformation from water to ice. To find the relationship between thermal conductivity and average temperature in both the frozen and unfrozen state, the x-axis was shifted by a temperature of +10.00 °C to artificially move all the x-axis values to be greater than zero. Figure 6 shows the variation of four substrates thermal conductivity with temperature (+10.001 °C) under different moisture content. A power function of the form of $y = A(T + 10.001)^B$ is found for wet samples. Fitting functions and coefficients of determination R^2 values are shown in Table 4, and these indicate that as moisture content increases, R^2 becomes closer to 1; when the substrate reaches its maximum moisture content, $R^2 = 0.99$.

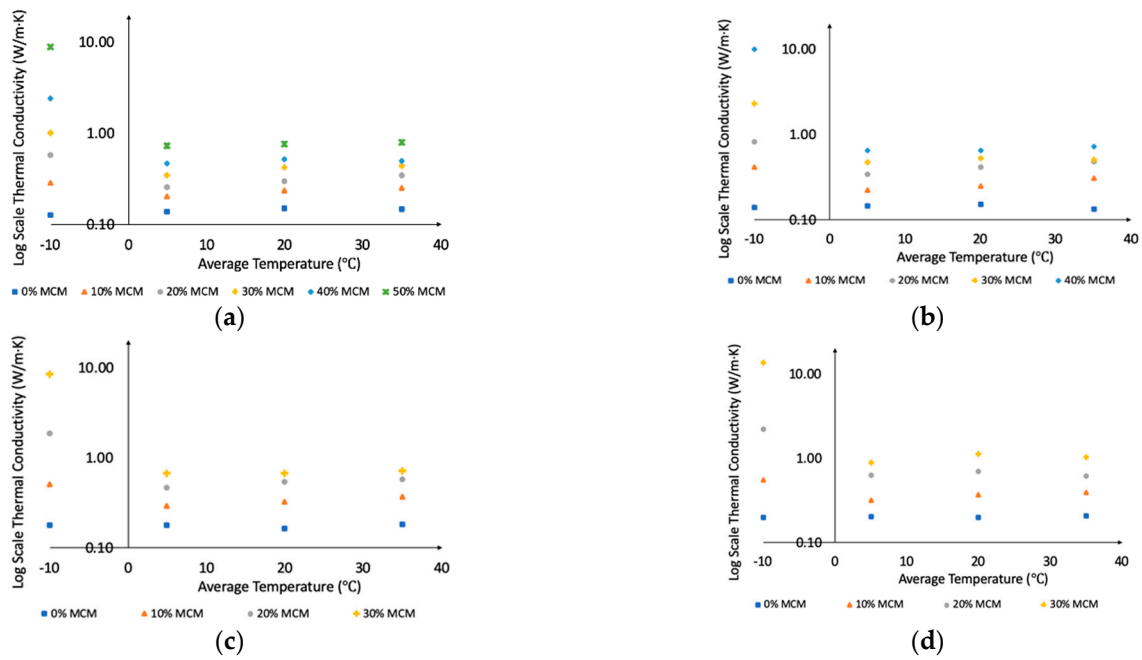


Figure 5. Thermal conductivity vs. average temperature at different moisture content for (a) Soprafloor I; (b) Zinco Blend; (c) Soprafloor X; (d) Eagle Lake.

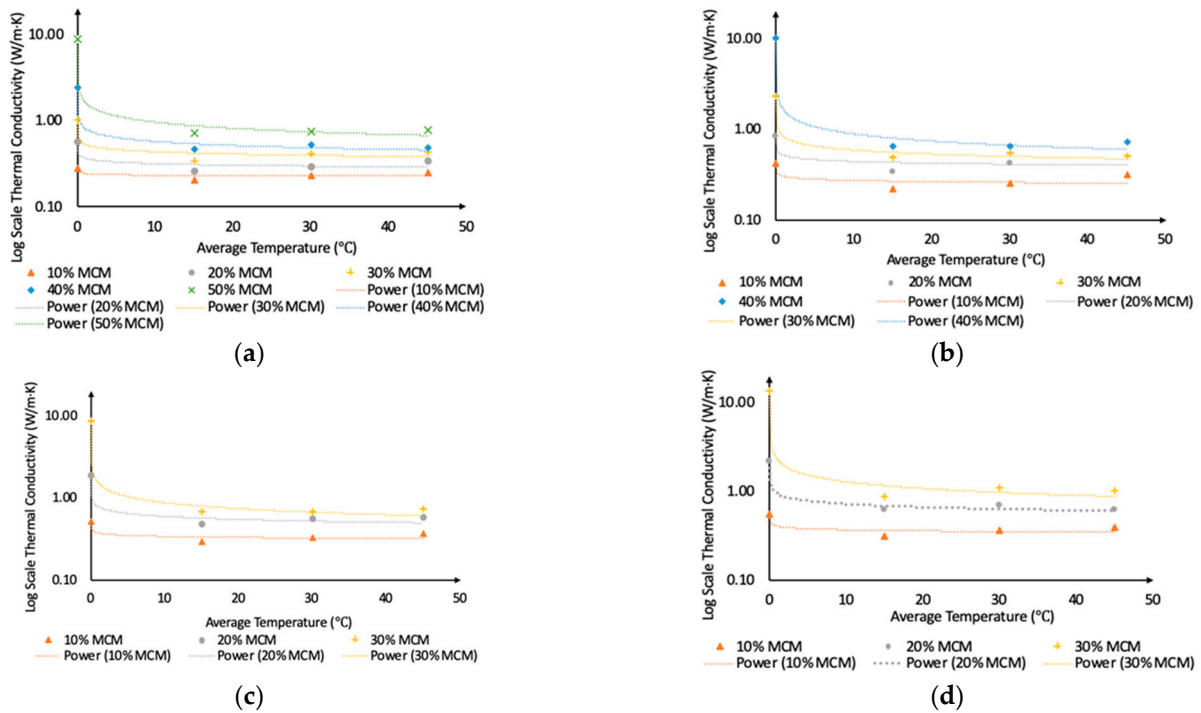


Figure 6. Thermal conductivity vs. average temperature (+10.001) at different moisture contents for (a) Soprafloor I; (b) Zinco Blend; (c) Soprafloor X; (d) Eagle Lake.

Table 4. Thermal conductivity y (W/m·K) as a function of x ($x = T + 10.001$).

	Sopraflor I	Zinco Blend	Sopraflor X	Eagle Lake
10%	$y = 0.25x^{-0.02}$ $R^2 = 0.56$	$y = 0.30x^{-0.05}$ $R^2 = 0.68$	$y = 0.37x^{-0.04}$ $R^2 = 0.75$	$y = 0.42x^{-0.41}$ $R^2 = 0.78$
20%	$y = 0.37x^{-0.06}$ $R^2 = 0.82$	$y = 0.52x^{-0.07}$ $R^2 = 0.79$	$y = 0.79x^{-0.12}$ $R^2 = 0.95$	$y = 0.95x^{-0.12}$ $R^2 = 0.98$
30%	$y = 0.54x^{-0.09}$ $R^2 = 0.91$	$y = 0.83x^{-0.15}$ $R^2 = 0.98$	$y = 1.54x^{-0.24}$ $R^2 = 0.99$	$y = 2.31x^{-0.25}$ $R^2 = 0.98$
40%	$y = 0.82x^{-0.15}$ $R^2 = 0.98$	$y = 1.63x^{-0.26}$ $R^2 = 0.99$	-	-
50%	$y = 1.67x^{-0.24}$ $R^2 = 0.99$	-	-	-

A two-way ANOVA analysis was used to further understand the main effects of moisture content and temperature, and their interaction on the substrate thermal conductivity. Data from all media types were combined to conduct the analysis but were divided between data observed when in the unfrozen state and data observed for all states (frozen and unfrozen). The analysis results (moisture content as 1 and average temperature as 2) in the unfrozen state ($f(2) = 0.659$, $p = 0.524$; $f(1) = 21.876$, $p \ll 0.001$) indicate that a significant (at the 5% level) effect of temperature on the substrate thermal conductivity is absent; whereas, the significant effect of moisture was identified, which is consistent with the detected significant trend of the substrate thermal conductivity over moisture by the Mann–Kendall test. The interaction effect of temperature and moisture on the thermal conductivity is not significant. Thus, in the unfrozen state and irrespective of media type, moisture content is the primary influential factor affecting substrate thermal conductivity. When combining the data collected in both the frozen and unfrozen states, the ANOVA results ($f(2) = 5.207$, $p = 0.003$; $f(1) = 5.528$, $p = 0.002$) show that the primary effects of both moisture and temperature are significant. In addition, a significant interaction effect of moisture and temperature was also detected ($f(2, 1) = 3.358$, $p = 0.003$). This significant effect of temperature and the significant interaction effect of temperature and moisture are expected given that temperature change is required in the water phase transition from liquid and solid, and vice-versa. Irrespective of the media type, the thermal conductivity largely increased in the frozen state from the unfrozen state (Figure 5), as solid water has higher thermal conductivity compared to liquid water.

3.2. Results of Energy Performance Experimental Study

3.2.1. Weather Data

Figure 7 shows the weather data from 30 May to 13 August, including air temperature, wind speed, humidity, and insolation collected from the weather station located on the roof of the University's David Turpin Building. From 30 May to 2 July 2, there was no rainfall and air temperature varied from 10.4 (at 06:17 on 30 May) to 22.7 °C (at 14:21 on 31 May). Humidity varied from 50.8% to 94.1%, the maximum insolation was 918.5 W/m² (at 13:56 on 1 June). From 9 July to 15 July, rainfall occurred from late 9 to 11 July, with peak precipitation of 5.33 mm at 23:00 on 9 July. Air temperature varied from 11.3 to 24.2 °C. Daily peak insolation occurred between 11:00 to 14:30. From 7 to 13 August, there was around 1 mm precipitation on 10 August. Air temperature varied from 13.6 (at 06:45 on 7 August) to 25.0 °C (at 18:18 on 7 August). Humidity varied from 48.6% to 97.0%. The maximum insolation was 929.1 W/m² (at 16:04 on 11 August). Evaporation data were computed based on the collected water mass data every day at 9:00 am using a handmade evaporation pan, evaporation results were 5.08 and 4.76 kg/(m²·day) for 7 and 8 August when the insolation was high. For 9 and 11 August, when average insolation decreased, evaporation data decreased to 2.70 and 2.42 kg/(m²·day), respectively. As for 10 August,

there was an increase in water in the pan by $0.14 \text{ kg}/(\text{m}^2 \cdot \text{day})$, but the evaporation was zero, this is due to rainfall on 10 August.

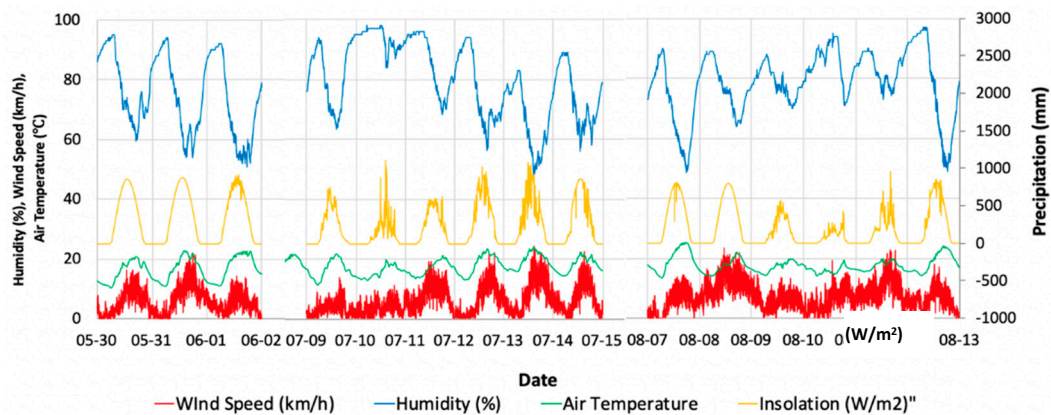


Figure 7. Weather data of 30 May–2 June; 9–14 July; 7–13 August.

The 1981–2010 Canadian Climate Normals [31] obtained for the Victoria International Airport indicate that the maximum and minimum average daily temperatures (\pm standard deviation of the average) for May to August are normally $7.2\text{--}16.9 \pm 1.0$, $9.8\text{--}19.9 \pm 0.9$, $11.3\text{--}22.4 \pm 0.9$, and $11.1\text{--}22.4 \pm 0.7$ °C, respectively; with rainfall in mm of 37.5, 30.6, 17.9, 23.8, respectively. Humidity averages around 60–80% for all four months. The weather data observed during the observation period are similar for temperatures and humidities to those provided by the 1981–2010 Canadian Climate Normals. The one difference is in the amount of precipitation observed. There was markedly less precipitation during the observation period than is normally experienced for this time of year. This essentially allowed for an observation reflective of temperature and humidity effects and not precipitation effects, which can adversely affect an experiment such as this one if not controlled.

3.2.2. Bare Roof (Test Cell A) vs. Roof with 150 mm thick Substrate (Test Cell B)

Data from the bare roof test cell and the roof with 150 mm thickness Sopraflor X test cell was collected in Victoria from 9–15 July 2019. Figure 8a shows the surface and indoor air temperature results of test cells A and B. The bare roof has a large temperature fluctuation between the day and night. In the daytime, with its roof surface black, the low albedo allows much (if not all) of the incoming solar radiation to be absorbed instead of being reflected. The daily maximum bare roof surface temperature is 1.95–2.87 times larger than the daily maximum ambient air temperature; but at night, the bare roof surface temperature is similar, and sometimes even lower than the outdoor air temperature. This is because of the heat convection with cool air that flows above the roof surface, and the sky longwave radiation [32]. It should be noted that the green roof with substrate only (no sedum mat) would also have a low albedo whereas the roof with a sedum mat would have a slightly higher albedo, thereby reflecting slightly more solar radiation than the other roofs, and therefore, there is less radiation available for absorption/transmittance for a roof with a sedum mat. While thermal conductivity, absorption and transmittance are independent of albedo, the slight differences in albedo between the roof surfaces tested suggest the need to compare interior and exterior temperatures as opposed to only exterior surface temperatures. Test cell B with 150 mm of substrate showed a significant temperature reduction, and a time delay in reaching peak temperatures when observing indoor air temperature as compared with test cell A. This is because the substrate layer acted as a thermal mass which stored heat in the daytime and released this heat to the ambient environment at night. This is also the reason why roof surface temperatures of cell B are higher than the outdoor air temperature at night.

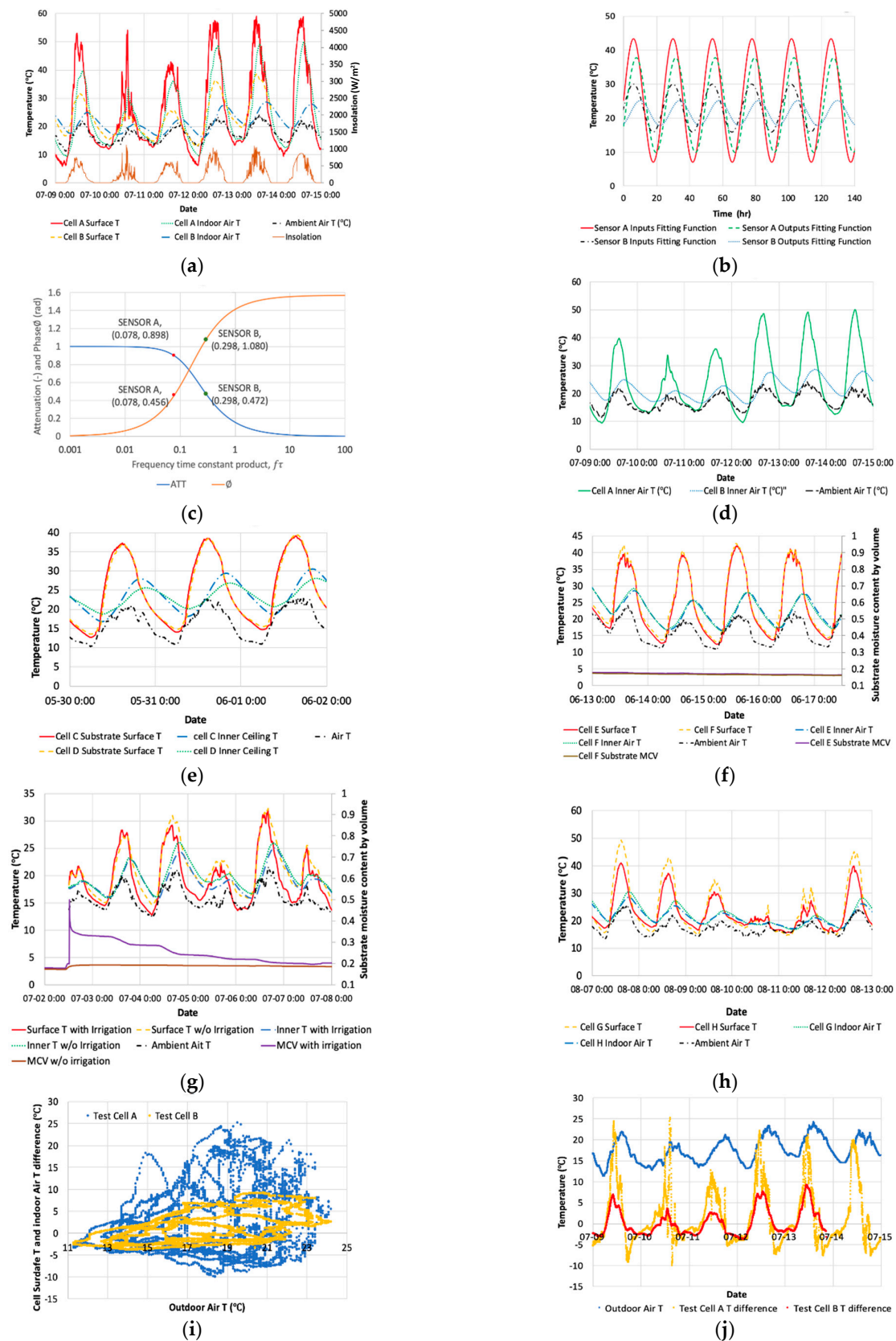


Figure 8. Temperature (T) results test cells (a) A and B; (b) functional plots of A and B; (c) attenuation and phase angle for A and B; (d) air temperature for A and B; temperature results for (e) C and D; (f) E and F before irrigation; (g) E and F after irrigation; (h) G and H; (i) surface and air T differences; (j) surface and indoor air T difference, outdoor air T vs. date.

To further analyze the thermal properties of the substrate layer, transient conduction and a lumped capacitance time constant [33] were analyzed. The lumped capacitance time constant is the amount of time for the sensor to respond to the thermal environment changes, it is the product of thermal capacitance of the sensor and the thermal resistance to heat transfer from the surface of the sensor. In this study, bare roof plywood ceiling together with EPDM pond liner were considered as sensor A, the 150 mm thick substrate layer, plywood ceiling, and EPDM pond liner were considered as sensor B. Surface temperatures of two test cells were considered as input. The indoor air temperature was considered as the output of two sensors. From Figure 8a we can see, both roof surface (input), and indoor air temperature (output) are following an oscillating function. The fitting functions of temperature ($^{\circ}\text{C}$) inputs and outputs for both sensors versus time (hours) were obtained using the excel solver method. Fitting functions and R^2 values are shown in Table 5 and plots of fitting functions are shown in Figure 8b. Since the inputs of the sensor followed an oscillating function, the attenuation of the amplitude of the oscillation (Att) and the phase lag (φ) can be calculated as following equations:

$$Att = \frac{1}{\sqrt{1 + (2\pi f\tau)^2}} \quad (5)$$

$$\varphi = \tan^{-1}(2\pi f\tau) \quad (6)$$

Table 5. Fitting functions of temperature inputs and outputs.

		Fitting Function	R^2
Sensor A (bare roof)	Input	$T = 18.15 \sin(0.2623t) + 25.205$	0.77
	Output	$T = 13.93 \sin(0.2628t - 0.456) + 23.845$	0.80
Sensor B	Input	$T = 5.27 \sin(0.2630t) + 22.960$	0.61
	Output	$T = 3.66 \sin(0.2629t - 1.080) + 21.516$	0.58

The frequency (f) and phase lag (φ) value can be achieved from Table 5, so the values of τ and attenuation were calculated based on equations above, and results are shown in Table 6. The results of phase angle and attenuation are also highlighted in Figure 8c. The lumped time constant for sensor A is 1.87 h, whereas the time constant for sensor B is 7.11 h. As discussed before, the time constant is the product of thermal capacitance and the thermal resistance; that is to say, the additional 150 mm thick substrate layer increases the total capacitance and thermal resistance, which makes the total time constant 3.8 times larger than that of the bare roof. The attenuation of the amplitude for sensor A and sensor B is 0.90 and 0.47, respectively. Due to thermal resistance, 150 mm substrate layer provided a 42.6% further reduction on the amplitude compared with that of the bare roof. The phase lag for sensor A and sensor B is 0.456 and 1.080 rad, respectively. Due to the thermal capacitance, the 150 mm substrate layer provided 0.624 rad further phase lag compared with that of the bare roof.

Table 6. Time constant results of two sensors.

	f (Cycles per Hour)	Time Constant τ (Hour)	$f \cdot \tau$	Att (-)	φ (Rad)
Sensor A	0.042	1.866	0.078	0.898	0.456
Sensor B	0.042	7.110	0.298	0.472	1.080

The relationship between test cell exterior and interior temperature vs. outdoor air temperature was analyzed, as shown in Figure 8i,j, and fitting functions of the two test cells are shown in Table 7. It can be seen from the table that, compared with the extensive roof (Test cell B), the bare roof (Test cell A) is influenced more by the outdoor air temperature.

This provides an explanation about the time constant results of test cell A (1.87 h) and test cell B (7.11 h).

Table 7. Functional forms for exterior–interior temperature difference vs. outdoor temperature.

System	Fitting Function	R ²
Test cell A (bare roof)	$T_{diff} = 0.62T_{OA} - 9.38$	0.07
Test cell B	$T_{diff} = 0.54T_{OA} - 9.20$	0.28

Figure 8d shows the test cells' inner ceiling temperature from 9–14 July. The variation of test cell A inner ceiling temperature is up to 38.7 °C, whereas the variation of test cell B inner ceiling temperature is 12.0 °C. Both test cells' inner ceiling temperature follows a sinusoidal function of the following form:

$$T = A_i \sin(\omega_i t - \varphi_i) + Tavg_i \quad (7)$$

where the ceiling temperature is T (°C), t is time in (hour) and i is either test cell A or B. Results of A , ω , φ , $Tavg$, and coefficients of determination R^2 of each day are shown in Table 8. Value A indicates the amplitude of the inner ceiling temperature and as we can see, the value of A_A is much higher than A_B . During the rainy days from 9–11 July, the amplitudes for both test cells were smaller than on dry days, which is determined by the solar radiation and outdoor temperature. Based on the results, one can see that no matter if the day is rainy or not, A_A is roughly four times larger than A_B . This means the 150 mm thick substrate layer provided better thermal protection against outdoor temperature and solar radiation. It had a 75% reduction in the amplitude of the inner ceiling temperature as compared with that of the bare roof test cell and kept the test cell B interior at a relatively steady state. Examining the results of angular frequency ω , the 150 mm thick substrate layer has a tiny positive influence on the value of angular frequency during rainy days, while during sunny days it has a slightly negative influence on the value of angular frequency. From the results of ω_B/ω_A , the substrate layer did not have a large influence on the frequency.

Table 8. Modelling parameters for bare roof vs. 150 mm test cells.

	Bare Roof (Cell A) vs. 150 mm (Cell B)					
	9 July	10 July	11 July	12 July	13 July	14 July
R_A^2	0.92	0.92	0.97	0.97	0.95	0.95
R_B^2	0.99	0.99	0.98	0.99	0.99	0.99
A_A	14.14	7.85	11.17	19.03	16.04	18.08
A_B	3.47	1.96	2.91	5.58	4.06	4.26
$(A_A - A_B)/A_A$	0.75	0.75	0.74	0.71	0.75	0.76
ω_A (rad/h)	0.30	0.28	0.29	0.28	0.30	0.30
ω_B (rad/h)	0.31	0.30	0.25	0.24	0.27	0.27
ω_B/ω_A	1.03	1.07	0.86	0.86	0.90	0.90
φ_A (rad)	2.89	2.89	2.96	2.86	2.84	2.88
φ_B (rad)	4.02	4.35	3.49	3.28	3.53	3.67
$(\varphi_B - \varphi_A)$	1.13	1.46	0.53	0.42	0.69	0.79
$Tavg_A$ (°C)	22.57	19.88	23.21	26.35	28.15	27.5
$Tavg_B$ (°C)	21.57	19.04	19.61	21.77	24.43	23.67
$(Tavg_A - Tavg_B)$	1.00	0.84	3.60	4.58	3.72	3.83

Results of φ shows the phase lag of two cells, which is due to the properties of thermal capacitance. The phase lag φ_A shows that no matter if on rainy or sunny days, the ceiling temperature delay for each day is always similar for the bare roof test cell, however, for cell B with the substrate, the phase lag is always larger than test cell A. The delay on rainy days becomes more significant. This is because substrate has a large thermal capacity which stores heat in the daytime and releases it to the ambient environment at night, and as

well, substrate thermal capacity increases as moisture content increases. T_{avg} shows the average inner ceiling temperature of the two cells. The bare roof shows a higher average temperature because of its black surface color, and the average temperature difference becomes larger on sunny days as outdoor insolation increases.

3.2.3. Extensive Roof (Test Cell C) vs. Intensive Roof (Test Cell D)

A test study of extensive and intensive substrate thermal performance was performed from 30 May to 2 June. Test cell C is the roof with 150 mm thick substrate, which is extensive, and test cell D is the roof with 200 mm thick substrate, which is intensive. Figure 8e shows the test cells' surface and inner ceiling temperatures from 30 May to 1 June. The surface temperature of the two test cells is always the same due to the same surface color and having the same components. The surface temperature varied from 12.6 to 39.4 °C, with daily peak surface temperature occurring between 13:00 to 16:00 when the insolation was high. As discussed before, because the substrate layer acted as a thermal mass, it released heat to the ambient at night which makes the surface temperature of the substrate higher than the ambient air temperature. As for the inner ceiling temperature of the two test cells, a significant reduction in temperature fluctuation and a delay in reaching the peak temperature occurred for both test cells. The ceiling temperature of test cell C varied from 16.8 to 30.5 °C, whereas for test cell D, it varied from 18.7 to 28.0 °C.

Following Equation (7), results of A , ω , φ , T_{avg} , and coefficients of determination R^2 of each day are shown in Table 9. Results for A show a further 40% reduction on the amplitude of the ceiling temperature of the cell with a 200 mm thick substrate compared with that of the cell with a 150 mm thick substrate; which in turn makes cell D's interior a relatively steady state. Results of ω shows the angular frequency of cell D is a little smaller than that of cell C, and the ratio between ω_C and ω_D were all close to 1. This means the thickness of the substrate does not have much of an influence on the angular frequency of the ceiling temperature. Results of phase lag φ indicates a more significant delay for test cell D. This is not surprising because the thermal capacity of substrate increases as the mass of the substrate increases. As for the average inner ceiling temperature T_{avg} , the difference between those two average temperatures is small and can be neglected. This is because those two test cells had the same outer surface temperature, and the thickness of the substrate will not influence the average ceiling temperature.

Table 9. Modeling parameters for 150 vs. 200 mm test cells.

	150 mm (Cell C) vs. 200 mm (Cell D)		
	30 May	31 May	1 June
R_C^2	0.99	0.98	0.99
R_D^2	0.99	0.99	0.99
A_C	5.36	5.37	5.68
A_D	3.28	3.22	3.55
$(A_C - A_D)/A_C$	0.39	0.40	0.37
ω_C (rad/h)	0.25	0.26	0.26
ω_D (rad/h)	0.24	0.25	0.24
ω_D/ω_C	0.94	0.96	0.95
φ_C (rad)	3.61	3.74	3.68
φ_D (rad)	3.65	3.84	3.75
$(\varphi_D - \varphi_C)$	0.04	0.10	0.07
T_{avgC} (°C)	22.26	23.57	24.38
T_{avgD} (°C)	22.22	23.46	24.35
$(T_{avgC} - T_{avgD})$	0.04	0.11	0.03

3.2.4. Roof with Irrigation (Test Cell E) vs. without Irrigation (Test Cell F)

A test study of substrate thermal performance at various moisture contents was performed from 2–8 July. Before the study, the two test cells were both covered with 150 mm thick substrate and left to rest for 2 weeks in July to make sure they were both

under the same initial conditions. Figure 8f shows the surface temperature, inner temperature, and substrate moisture content of the two test cells before irrigation (with the same initial conditions).

Fifteen liters of water were added to test cell E on 2 June, and Figure 8g shows the temperature and moisture content variation of test cells E and F after irrigation. For the substrate moisture content, before irrigation the two cells had the same moisture content: 17.5%. After irrigation, cell E's substrate moisture content increased from 18% to 49.9% suddenly and dropped gradually until it reached a constant value at around 20% on 7 July. For the substrate surface temperature, the surface temperature of the two test cells started to behave differently after 6 h of irrigation. At night, cell E's surface temperature is 1.5–4 °C lower than that of test cell F. Cell E's maximum surface temperature on 4 and 5 June is 1.4–1.9 °C lower than cell F.

Table 10 shows the fitting function of the two cells' surface and indoor temperature. For the test cell with irrigation, the amplitude of the inner temperature had a 54% reduction compared with that of the surface temperature, while for the test cell without irrigation, the amplitude of inner temperature had a 46% reduction compared with that of surface temperature. This is because for the substrate with irrigation, part of the energy absorbed by the substrate was released by evaporation, which decreases the energy transferred to the interior. Based on the phase parameter of the fitting function, the phase lag of the test cell with irrigation is higher due to the increase of heat capacity when water was added to the substrate.

Table 10. Fitting functions of surface and indoor air T of test cells E and F.

		Fitting Function	R ²
Test cell E (with irrigation)	Surface T	$T = 5.65 \sin(0.263t) + 19.03$	0.69
	Indoor air T	$T = 2.60 \sin(0.265t - 1.256) + 18.84$	0.51
Test cell F (no irrigation)	Surface T	$T = 4.91 \sin(0.264t) + 20.64$	0.58
	Indoor air T	$T = 2.63 \sin(0.265t - 0.989) + 19.48$	0.45

3.2.5. Roof without Vegetation (Test Cell G) vs. Roof with Vegetation (Test Cell H)

A test study of green roof thermal performance with or without a vegetation layer was performed from 7 to 13 August. To study the thermal performance of green roof with or without vegetation layer, a layer of sedum mat was placed on the top of test cell H. The substrate surface and inner air temperature results of the two test cells are shown in Figure 8h. Substrate surface temperature of cell G varied from 14.4 to 49.2 °C while that of cell H varied from 16.6 to 40.9 °C. Temperature variation of the cell with the sedum mat is more stable compared with that of the cell without a sedum mat. When the insolation is high, because of its color and foliage shading effect, the vegetation layer provided more opportunity for transpiration and protection against solar radiation, which decreased the substrate maximum surface temperature by 8.3 °C. Following Equation (7), results of A , ω , φ , T_{avg} , and coefficients of determination R^2 of each day are shown in Table 11.

Temperature data on 10 August did not follow a sine trend. The R^2 values of the two test cells on 10 August are 0.87 and 0.85, which is much lower than the other days, and thus, data of 10 August was excluded from this modeling. Based on the results of value A , it can be seen that on the dates of the 7th, 8th and 10th of August, when the insolation is high, both cells had high amplitudes compared with the other days. The test cell with the sedum mat had a 25% reduction in the amplitude of the inner air temperature as compared to the cell without a sedum mat. From the results of ω_H/ω_G , the vegetation layer did not have a strong influence on the value of angular frequency. For the phase lag φ of the two cells, the phase lag of the test cell without the sedum mat was only 0.05–0.10 times larger than that of the cell with the vegetation layer. This difference is small because the delay is mostly determined by the thermal capacity of the substrate layer and both cells had the same amount of substrate, so the phase lag of the two cells inner air temperature is very similar. The inner air temperature of the cell with sedum mat on was 0.12–0.72 °C

lower than that without the sedum mat on. Issa et al. [19] also showed similar results and conclusions. In their research they found that the control roof had the largest day and night indoor temperature fluctuations as compared with a sand roof and a silt clay roof because the substrate layer acted as a thermal mass. Additionally, compared with the with nonvegetated roof, the inner temperature of the vegetated roof dropped considerably.

Table 11. Modeling parameters for nonvegetated and vegetated test cells.

	No Veg. (Cell G) vs. with Veg. (Cell H)					
	7 August	8 August	9 August	10 August	11 August	12 August
R_G^2	0.99	0.99	0.99	0.87	0.98	0.97
R_H^2	0.99	0.99	0.99	0.85	0.98	0.98
A_G	5.11	3.72	2.48	33.21	2.49	5.4
A_H	3.95	2.78	1.91	30.98	1.9	4.34
$(A_G - A_H)/A_G$	0.23	0.25	0.23	0.07	0.24	0.20
ω_G (rad/h)	0.28	0.293	0.285	0.029	0.24	0.235
ω_H (rad/h)	0.283	0.299	0.285	0.025	0.249	0.234
ω_H/ω_G	1.01	1.02	1.00	0.86	1.04	1.00
φ_G (rad)	3.82	4.02	4.11	2.03	3.17	3.09
φ_H (rad)	3.77	4.01	4	1	3.17	3.01
$(\varphi_H - \varphi_G)$	-0.05	-0.01	-0.11	-1.03	0.00	-0.08
$Tavg_G$ (°C)	24.81	22.97	21.06	51.7	19	22.05
$Tavg_H$ (°C)	24.18	22.38	20.79	49.69	18.88	21.33
$(Tavg_G - Tavg_H)$	0.63	0.59	0.27	2.01	0.12	0.72

All experiments like these (both the laboratory experiments and the outdoor experiments) are subject to errors arising from instrumentation and experimental design. In terms of instrumentation, all instrument errors used in this research were small in comparison to the errors incurred through the experimental designs. It is not believed that instrument errors were significant enough to affect inferences and conclusions in this work. The errors arising from experimental design, however, involve site specificity (conditions specific to the location) and scale (the physical size of the samples). Both, if significant, can minimize the capacity of results to be used at other locations and other points in time. To deal with the site specificity, one can avoid looking at absolute values. It is for this reason that the authors compared the relative differences between interior and exterior temperatures, relative responses across samples and cells, and modeled all cells with the same first-order dynamic system, which further facilitated internal comparisons. Relative comparisons avoid the pitfalls and errors associated with absolute comparisons. Scale effects are real and present in any experiment in which a dynamic similitude is not considered. The small, outdoor test cells were designed to a scale that was practical given spatial, logistic and financial constraints. Scale effects in such situations are primarily seen at the edges, or physical borders, of the system being scaled. For this reason, the authors placed the temperature sensors as closely as possible to the centroid of the cells and as far away from the edges as possible. Edge effects are still possible in this small a system, but their effects are minimized as much as physically possible given the placement of the sensors. Validation and quantification of errors arising from scale are outside the scope of this work and recommended for future work.

4. Conclusions

Results of the experimental study into the thermal conductivity at different temperature and moisture contents show that at the same temperature and moisture content, Eagle Lake has the highest thermal conductivity while Sopraflor I has the lowest thermal conductivity. It appears, based on the results available from this study, irrespective of temperature or moisture content, the substrate with higher dry density has higher thermal conductivity. This is consistent with the test performed by Barozzi et al. [34]. More research should be performed, however, to further study the relationship between dry density and thermal conductivity for other substrates, as porosity also influences substrate dry density and thermal conductivity. With temperature change and in an unfrozen state, the

Mann–Kendall trend test (M-K test) showed there is no significant relationship between thermal conductivity and temperature. An ANOVA test was also applied given the low number of data points used in the M-K test and the ANOVA results confirmed this outcome. Results from Zhang et al. [20] also showed that for the thawed substrates, the influence of temperature on the thermal conductivity can be neglected, while in the phase transition zone, thermal conductivity increases significantly as temperature decreases to below zero. This was also observed when combining all data in both frozen and in unfrozen states. In the phase transition zone (between +5 and -10 °C), as temperature decreases, thermal conductivity increases sharply during the transition from water to ice because of the difference in thermal conductivity difference between the two phases. In general, when in the unfrozen state and as moisture content changed, thermal conductivity increased linearly as moisture content increased. Clarke et al. [29] also showed a simple linear regression fit for the thermal conductivity of three different substrates as a function of moisture content. In the frozen state, however, an exponential function exists between thermal conductivity and substrate moisture content prior to freezing.

Results of the experimental study on the substrate thermal performance show that bare roofs and extensive roofs act very differently in terms of response to changes in outdoor temperature. Roof albedo affects the amount of solar radiation available for absorption/transmittance, and the bare roof, which had the lowest albedo of all tested roofs, would be subject to greater heating than the green roofs, which have slightly higher albedos (although only marginally higher). Beyond the amount of solar radiation absorbed, a roof's response to outdoor temperature is then dictated by the thermal conductivity of the roof layer as a whole. As outdoor temperature fluctuated sinusoidal each day, it was found that compared with the bare roof, the extensive roof has 75% reduction on the amplitude of the interior temperature. Compared to the extensive roof, there is a further 40% reduction in the amplitude of the interior by the intensive roof. In addition, interior temperature decreased when irrigated as compared to conditions without irrigation. When a sedum mat was added above the substrate, there was a 20% reduction in the amplitude of the interior temperature compared with the cell without the sedum mat.

All of these results point to the need to consider both moisture effects and seasonal variability in the design and maintenance of green roofs. The laboratory experiment examining the relationship between moisture content and thermal conductivity and provided mathematical functions for thermal conductivity as a function of moisture content for frozen and non-frozen conditions (seen in Table 3). Energy transfer models of actual green roofs that currently use static values of thermal conductivity can now simply modify the thermal conductivity as a simple mathematical function of moisture content. Additionally, mathematical functions were found that neatly related thermal conductivity as a function of temperature when temperature moved from a frozen to a non-frozen state. These can provide information on how to parameterize thermal conductivity for a green roof in the winter time when conducting energy and temperature simulations for a building with a green roof.

The outdoor, small test cells were useful because they allowed for a clear understanding of the effects of the studied substrates, and the potential for vegetation, on modulating interior temperature in comparison to bare roofs. By reducing the roof to a first-order dynamic system—effectively a one parameter (τ), black-box—comparisons could be made between roofs more simply. Each roof's behavior was reduced to values of τ and changes in temperature amplitude and phase. By simply expressing the interior temperatures as the same sinusoidal functions but with different amplitudes and phases, one can use these simple black box models to illustrate the importance of certain design parameters over others in designing a green roof. In this study, this black-box modeling showed that any green roof is a marked improvement in insulative value over no green roof, but the extra 50 mm of substrate thickness was marginally helpful, and thus, the thinner, extensive green roof is sufficient. Similarly, the results showed that incorporating changes in moisture

content either through irrigation or rainfall is an important consideration in modelling or predicting interior air temperatures.

Understanding these important effects on thermal balance can facilitate resilient responses to climate change by affecting how we design green roofs. Future research extending this work should consider scale effects due to the size of the test cells used outdoors; observations taken over a greater range of temperature changes including sub-zero temperatures; modeling outdoor green roofs to include a dynamic thermal conductivity as a function of moisture content in energy budget models.

Author Contributions: Conceptualization, P.M. and C.V.; Methodology, B.S., P.M., C.V. and J.H.; Validation, B.S.; Formal Analysis, B.S.; Investigation, B.S.; Resources, P.M., C.V. and J.H.; Data Curation, B.S.; Writing—Original Draft Preparation, B.S.; Writing—Review and Editing, B.S., C.V., P.M. and J.H.; Supervision, C.V., P.M. and J.H.; Project Administration, C.V., P.M. and J.H.; Funding Acquisition, C.V. and P.M. All authors have read and agreed to the published version of the manuscript.

Funding: This research was supported with funds from CFI-JELF 32294, NSERC RGPIN-2015-05096 and from Homeowner Protection Office, Branch of BC Housing-2015-35622.

Acknowledgments: The authors would like to thank the Reviewers for their insightful comments, which greatly improved the paper. We would also like to thank Yao Zhao of Nanjing Forestry University in China and University of Victoria, and Civil Engineering lab staff members Armando Tura and Geoff Burton for their help in this research. Thanks are also due to the University of Calgary and the City of Calgary for providing substrate samples.

Conflicts of Interest: The authors declare no conflict of interest.

References

- Pérez-Lombard, L.; Ortiz, J.; Pout, C. A review on buildings energy consumption information. *Energy Build.* **2008**, *40*, 394–398. [CrossRef]
- Valipour, M. Land use policy and agricultural water management of the previous half of century in Africa. *Appl. Water Sci.* **2014**, *5*, 367–395. [CrossRef]
- Mahmoodzadeh, M.; Mukhopadhyaya, P.; Valeo, C. Effects of Extensive Green Roofs on Energy Performance of School Buildings in Four North American Climates. *Water* **2019**, *12*, 6. [CrossRef]
- Sha, M.; Kim, R.; Ra, M. Green roof benefits, opportunities and challenges—A review. *Renew. Sustain. Energy Rev.* **2018**, *90*, 757–773.
- Fioretti, R.; Palla, A.; Lanza, L.; Principi, P. Green roof energy and water related performance in the Mediterranean climate. *Build. Environ.* **2010**, *45*, 1890–1904. [CrossRef]
- Pianella, A.; Clarke, R.E.; Williams, N.S.; Chen, Z.; Aye, L. Steady-state and transient thermal measurements of green roof substrates. *Energy Build.* **2016**, *131*, 123–131. [CrossRef]
- Liu, R.; Stanford, R.L. The influence of extensive green roofs on rainwater runoff quality: A field-scale study in southwest China. *Environ. Sci. Pollut. Res.* **2020**, *27*, 12932–12941. [CrossRef]
- United States General Services Administration. A Report of the Benefits and Challenges of Green Roofs on Public and Commercial Buildings. Washington, DC, Maryland, USA. May 2011. 152 Pages. Available online: https://www.gsa.gov/cdnstatic/The_Benefits_and_Challenges_of_Green_Roofs_on_Public_and_Commercial_Buildings.pdf (accessed on 5 April 2021).
- Berardi, U.; GhaffarianHoseini, A.; GhaffarianHoseini, A. State-of-the-art analysis of the environmental benefits of green roofs. *Appl. Energy* **2014**, *115*, 411–428. [CrossRef]
- Cook-patton, S.C.; Bauerle, T.L. Potential benefits of plant diversity on vegetated roofs: A literature review. *J. Environ. Manag.* **2012**, *106*, 85–92. [CrossRef]
- Gabrych, M.; Kotze, D.J.; Lehvävirta, S. Substrate depth and roof age strongly affect plant abundances on sedum-moss and meadow green roofs in Helsinki, Finland. *Ecol. Eng.* **2016**, *86*, 95–104. [CrossRef]
- Farrell, C.; Mitchell, R.; Szota, C.; Rayner, J.; Williams, N. Green roofs for hot and dry climates: Interacting effects of plant water use, succulence and substrate. *Ecol. Eng.* **2012**, *49*, 270–276. [CrossRef]
- Teeri, J.A.; Turner, M.; Gurevitch, J. The Response of Leaf Water Potential and Crassulacean Acid Metabolism to Prolonged Drought in Sedum rubrotinctum. *Plant Physiol.* **1986**, *81*, 678–680. [CrossRef]
- Durhman, A.K.; Rowe, D.B.; Rugh, C.L. Effect of Substrate Depth on Initial Growth, Coverage, and Survival of 25 Succulent Green Roof Plant Taxa. *HortScience* **2007**, *42*, 588–595. [CrossRef]
- Vijayaraghavan, K. Green roofs: A critical review on the role of components, benefits, limitations and trends. *Renew. Sustain. Energy Rev.* **2016**, *57*, 740–752. [CrossRef]

16. Vera, S.; Pinto, C.; Tabares-Velasco, P.C.; Bustamante, W.; Victorero, F.; Gironás, J.; Bonilla, C.A. Influence of vegetation, substrate, and thermal insulation of an extensive vegetated roof on the thermal performance of retail stores in semiarid and marine climates. *Energy Build.* **2017**, *146*, 312–321. [[CrossRef](#)]
17. Narsilio, G.A.; Kress, J.; Sup, T. Computers and Geotechnics Characterisation of conduction phenomena in soils at the particle-scale: Finite element analyses in conjunction with synthetic 3D imaging. *Comput. Geotech.* **2010**, *37*, 828–836. [[CrossRef](#)]
18. Yun, T.S.; Santamarina, J.C. Fundamental study of thermal conduction in dry soils. *Granul. Matter* **2008**, *10*, 197–207. [[CrossRef](#)]
19. Issa, R.J.; Leitch, K.; Chang, B. Experimental Heat Transfer Study on Green Roofs in a Semiarid Climate during Summer. *J. Constr. Eng.* **2015**, *2015*. [[CrossRef](#)]
20. Zhang, M.; Lu, J.; Lai, Y.; Zhang, X. Variation of the thermal conductivity of a silty clay during a freezing-thawing process. *Int. J. Heat Mass Transf.* **2018**, *124*, 1059–1067. [[CrossRef](#)]
21. Hill, J.; Drake, J.; Sleep, B. Comparisons of extensive green roof media in Southern Ontario. *Ecol. Eng.* **2016**, *94*, 418–426. [[CrossRef](#)]
22. Kottek, M.; Grieser, J.; Beck, C.; Rudolf, B.; Rubel, F. World Map of the Köppen-Geiger climate classification updated. *Meteorol. Z.* **2006**, *15*, 259–263. [[CrossRef](#)]
23. ASTM E2399-05. *Standard Test Method for Maximum Media Density for Dead Load Analysis of Green Roof Systems*; ASTM: West Conshohocken, PA, USA, 2017; pp. 1–4.
24. ASTM C687-96. *Standard Practice for Determination of Thermal Resistance of Loose-Fill Building*. *Significance* **2003**, *4*, 1–11.
25. ASTM D698-07. *Standard Test Methods for Laboratory Compaction Characteristics of Soil Using Standard Effort (12,400 ft-lbf/ft³ (600 kN-m/m³))*; ASTM Int.: West Conshohocken, PA, USA, 2016; Volume 3, pp. 1–13.
26. Clarke, R.E. Flexible Buffer Materials to Reduce Contact Resistance in Thermal Insulation Measurements. In *Proceedings of the 32th International Thermal Conductivity Conference and 20th International Thermal Expansion Symposium*; Purdue University Scholarly Publishing Services: West Lafayette, IN, USA, 2014.
27. ASTM C518-98. *Standard Test Method for Steady-State Thermal Transmission Properties by Means of the Heat Flow Meter Apparatus*; ASTM: West Conshohocken, PA, USA, 2011; Volume 4, pp. 1–10.
28. Denner, T. *Operating Instructions Heat Flow Meter HFM 436/3 Lambda*; NETZSCH: Selb, Germany, 2014.
29. Clarke, R.E.; Pianella, A.; Shabani, B.; Rosengarten, G. Steady-state thermal measurement of moist granular earthen materials. *J. Build. Phys.* **2016**, *41*, 101–119. [[CrossRef](#)]
30. Akther, M.; He, J.; Chu, A.; Valeo, C.; Khan, U.T.; van Duin, B. Response of green roof performance to multiple hydrologic and design variables: A laboratory investigation. *Water Sci. Technol.* **2018**, *77*, 2834–2840. [[CrossRef](#)] [[PubMed](#)]
31. 1981–2010 Canadian Climate Normals, Environment and Natural Resources, Government of Canada. Available online: climate.weather.gc.ca/climate_normals/index_e.html (accessed on 5 April 2021).
32. Jiang, L.; Tang, M. Thermal analysis of extensive green roofs combined with night ventilation for space cooling. *Energy Build.* **2017**, *156*, 238–249. [[CrossRef](#)]
33. Nellis, G.; Klein, S. *Heat Transfer*; Cambridge University Press: NY, NY, USA, 2009. [[CrossRef](#)]
34. Barozzi, B.; Bellazzi, A.; Maffè, C.; Pollastro, M. Measurement of Thermal Properties of Growing Media for Green Roofs: Assessment of a Laboratory Procedure and Experimental Results. *Buildings* **2017**, *7*, 99. [[CrossRef](#)]